ACS APPLIED MATERIALS & INTERFACES

Research Article

Cite This: ACS Appl. Mater. Interfaces 2020, 12, 1292−1298

www.acsami.org

Plasmonically Enhanced Upconversion Luminescence via Holographically Formed Silver Nanogratings

Anshi Chu,[†,‡,⊥] Huilin He,[‡,§,⊥] Zhen Yin,[‡] Ruiheng Peng,[‡] Hongcheng Yang,[‡] Xian Gao,[‡] Dan Luo,[‡] Rui Chen,[‡] Guichuan Xing,*[,∥] and Yan Jun Liu*[,‡]

[†]Key Laboratory of Flexible Electronics (KLOFE) & Institute of Advanced Materials (IAM), Jiangsu National Synergetic Innovation Center for Advanced Materials (SICAM), Nanjing Tech University (NanjingTech), Nanjing 211816, China

[‡]Department of Electrical and Electronic Engineering, Southern University of Science and Technology, Shenzhen 518055, China

[§]Harbin Institute of Technology, Harbin 150001, China

[∥]Institute of Applied Physics and Materials Engineering, University of Macau, Macau SAR 999078, China

Supporting Information

ABSTRACT: Greatly enhanced upconversion luminescence was demonstrated by integrating the core−shell upconversion nanorods with the Ag nanogratings. Both the Ag nanogratings and upconversion nanorods were fabricated/synthesized in a facile, cost-effective, high-throughput way. Experimental results showed that the upconversion luminescence intensity of Er^{3+} in the core−shell upconversion nanorods can be well tuned and enhanced by changing the shell thickness and the period of the Ag nanograting. The underlying physical mechanism for the upconversion luminescence enhancement was attributed to the plasmonically enhanced near infrared broadband absorption of the periodic Ag nanograting and the localized surface plasmon resonance of Ag nanocrystals. The maximum enhanced factors of 523 nm, 544 nm (green emission), and 658 nm (red emission) of Er^{3+} ions excited at 980 nm are 3.8-, 5.5-, and 4.6-folds, respectively. Our fabrication approach and results suggest that such a simple integration is potentially useful for biosensing/imaging and anti-counterfeiting applications.

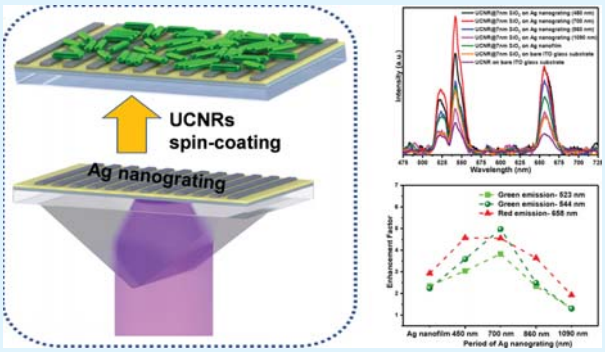

KEYWORDS: *holographical synthesis, nanograting, plasmonic enhancement, upconversion, core−shell nanorod*

INTRODUCTION

Photon upconversion, a process that converts low-energy excitation light (e.g., the near infrared (NIR)) into high-energy emission (e.g., ultraviolet, visible, or NIR), has long been a topic of great interest in optics. Due to their excellent photostability, large anti-Stokes shift, narrowband emission, and long excited-state lifetime, upconversion nanoparticles (UCNPs) have shown a wide range of potential applications in bioimaging, therapeutics, anti-counterfeiting, and photovoltaic devices.[1−5] However, their low upconversion luminescence (UCL) efficiency is still one of the limiting factors for their further potential applications. Up to now, various approaches have been explored to enhance the UCL, including the design of core−shell structures, energy transfer (ET) modulation, photonic crystal engineering, and plasmonic enhancement.[5−12] Among them, plasmon-enhanced upconversion is a challenging yet exciting research field from the perspectives in both fundamentals and applications. Surface plasmons enable the manipulation of light−matter interactions at the nanoscale, providing an efficient approach to improve the UCL efficiency.[5,9−21] In general, the principle strategy of surface plasmon enhancing UCL is to tune the plasmonic resonance to overlap with the absorption or emission band to achieve the plasmonically enhanced absorption or emission. For instance, the plasmonic resonances of Ag nanoparticles can be easily tuned in the visible range via controlling their morphology and size to achieve plasmon-enhanced emission of UCNPs.[10,11,16] Random patterns,[17,18] such as disordered Ag nanoparticles array and Ag nanowire network structures fabricated via a chemical way, have also been investigated with their absorption extended to the NIR range to enhance the absorption of NIR excitation of UCNPs. With advanced nanofabrication techniques, a variety of Ag periodic patterns[20,21] have been fabricated to achieve the angle-dependent or excitation power density-dependent UCL enhancement from the Ag gratings. Furthermore, their fabrication is costly, labor-intensive, process-complicated, and time-consuming.

In this work, we demonstrate a facile and cost-effective photochemical method to holographically synthesize Ag nanogratings, which is further utilized to enhance UCL of

Received: September 11, 2019
Accepted: December 10, 2019
Published: December 10, 2019

DOI: 10.1021/acsami.9b16461
ACS Appl. Mater. Interfaces 2020, 12, 1292−1298

core−shell upconversion nanorods (UCNRs). The period of the Ag nanograting can be easily tuned, leading to a tunable NIR broadband absorption from 850 to 1300 nm that can effectively match the absorption cross section of the sensitizer Yb^{3+} ions in the UCNRs. By synergizing the localized surface plasmon resonance (LSPR) of Ag nanocrystals and the Ag nanograting-coupled surface plasmon resonances, the plasmon-induced UCL enhancement is studied by integrating the core−shell UCNRs with the Ag nanogratings. The UCL enhancement is highly dependent on the shell thickness of the core−shell UCNRs and the period of Ag nanograting. The achieved enhancement factors (EFs) of 523 nm, 544 nm (green emission), and 658 nm (red emission) of Er^{3+} ions are 3.8, 5.5, and 4.6, respectively. Our facile, cost-effective, high-throughput approach makes the enhanced UCL potentially useful for biosensing/imaging and anti-counterfeiting applications.

EXPERIMENTAL SECTION

Chemical Reagents. All the rare-earth chloride $RECl_3$ (RE^{3+} = Y^{3+}, Gd^{3+}, Yb^{3+}, and Er^{3+}) (99.99% purity) was purchased from Alfa Aesar. Silver nitrate ($AgNO_3$) and trisodium citrate dihydrate ($C_6H_5Na_3O_7{\cdot}2H_2O$) were purchased from Sinopharm Chemical Reagent Co., Ltd. Oleic acid, ammonium fluoride (NH_4F), cyclohexane, Igepal co-520 ($(C_2H_4O)_n{\cdot}C_{15}H_{24}O$, $n \sim 5$), and tetraethyl orthosilicate (TEOS) were purchased from Aladdin Industrial Corp. Ethanol, ammonium hydroxide (NH_4OH), and acetone were purchased from Shanghai Lingfeng Chemical Reagent Co., Ltd. Sodium hydroxide (NaOH) was purchased from Shanghai Macklin Biochemical Co., Ltd. Polyimide resin (ZKPI-410, 5−6%) was purchased from POME Co., Ltd. All the chemicals were of analytical grade and used as received without further purification.

Preparation of Ag Nanograting and Nanofilm. The Ag nanograting and nanofilm were synthesized via a modified photochemical method based on the previous report.[22,23] An argon ion laser (363 nm) was utilized as the light source with an output power of 0.18 W. The laser beam was collimated by an expander system and then divided into two separate ones by impinging it onto the apex of a prism. These two separate beams intersect at the base of the prism and interfere each other to form a stable fringe pattern. As shown in Figure 1, an indium tin oxide (ITO) glass substrate was spin-coated with a uniform layer of polyimide, treated with UV ozone, and then placed on the base surface of the inverted prism (Scheme I in Figure 1). Two hundred microliters of mixed solution consisting of the 100 μL of silver nitrate solution (0.01 M) and 100 μL of sodium citrate solution (0.01 M) was drop-casted and spread on the polyimide layer. Under the exposure of the UV laser interference pattern, photochemical reduction took place in the solution. The Ag nanogratings were holographically synthesized with a laser irradiation of ∼30 min. In a similar fashion, the Ag nanogratings with different periods were fabricated by simply changing the prisms with different apex angles. Meanwhile, the Ag nanofilm can be easily synthesized with the similar setup by just removing the prism (Scheme II in Figure 1).

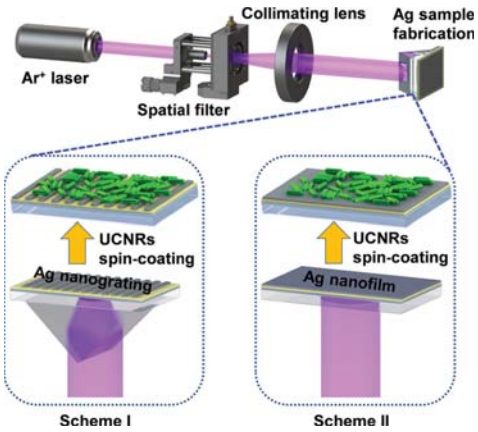

Figure 1. Schematic fabrication process of silver nanograting (Scheme I) and nanofilm (Scheme II).

Synthesis of UCNRs. UCNRs were synthesized via a mild hydrothermal method reported before.[24] NaOH (1.5 g) was dissolved in 7.5 mL of deionized water, and 25 mL of ethanol and 25 mL of oleic acid were added in sequence under continuous stirring. $RECl_3$ (2 mmol, RE = Y, Yb, Er, and Gd) and NH_4F (5 mL, 2 M) were added into the mixture. The above solution was transferred to a 100 mL stainless Teflon-lined autoclave, kept at 200 °C for 2 h, and then naturally cooled down to room temperature. The UCNRs obtained by the reaction were collected by centrifugation, washed successively with deionized water and ethanol three times, and then dispersed in cyclohexane for use.

Synthesis of Core−Shell UCNRs. The synthesis of SiO_2 shell coating on the synthesized UCNRs was based on the modified Stöber method[25] with TEOS as the silica precursor. First, 20 mg of the synthesized UCNRs and 5 mL of cyclohexane were added into a 20 mL scintillation vial and ultrasonically dispersed for 20 min. Second, 0.1 mL of Igepal and 6 mL of cyclohexane were added into the vial and stirred for 10 min. Third, 0.4 mL of Igepal and 0.08 mL of NH_4OH were added into the solution and sonicated for another 20 min until the solution became transparent. Finally, to achieve desired SiO_2 shell thickness, different amounts (0.01, 0.02, 0.04, 0.08, and 0.16 mL) of TEOS were added into the vial and the solution was stirred for 48 h. The UCNR@SiO_2 was precipitated using acetone, centrifuged, and washed with a mixture of ethanol/water (1:1) for several times and dispersed in ethanol.

Core−Shell UCNR Deposition. Core−shell UCNR solution (20 μL, 1 mg/mL) was spin-coated on the Ag nanogratings with the four different periods, Ag nanofilm, and bare ITO glass substrate for the UCL test.

Characterization. The crystalline structures of nanocrystals were characterized by X-ray diffraction (XRD) in a D8 Advance X-ray diffractometer (Bruker) at a scanning rate of 0.2 °/min with a Cu Kα radiation (151.54056 Å). The morphology, size distribution, and composition of as-prepared nanocrystals were investigated by the field emission scanning electron microscopy (FESEM, Merlin, Zeiss) at an acceleration voltage of 5 kV and high-resolution transmission electron microscopy (HR-TEM, Talos F200X, FEI) operating at 200 kV with an energy-dispersive X-ray spectrometer (EDS). For the top-view SEM observation, the fabricated Ag nanogratings can be tested directly due to their good conductivity. For cross-sectional SEM observation, the samples were prepared by the following subsequent steps: the glass from the back of the samples was cut using a diamond cutter, they were put into the liquid nitrogen for several minutes, they were broke along the cutting line, and finally, the Pt was coated onto the cross section of the sample for SEM observation. The TEM samples were prepared by dropping the dispersed sample solution (1 mg/mL) onto a 200 mesh carbon-coated copper grid followed by the evaporation of solvent. The absorption spectrum was tested by a UV−vis−NIR microspectrophotometer (508PV, CRAIC). Dynamic light scattering (DLS) and zeta potential data were acquired on a Zetasizer Nano ZSE (Malvern). Thermogravimetric analysis (TGA) was conducted using a TGA/DSC1 (Mettler Toledo) at a heating rate of 10 °C/min under an air atmosphere. Fourier transform infrared (FTIR) spectra were collected in the transmission mode via an IRTracer-100 FTIR spectrometer (SHIMADZU) using the KBr method. X-ray photoelectron spectroscopy (XPS) was recorded using an ESCALAB 250Xi spectrophotometer (Thermo Fisher). The upconversion emission spectra were recorded by a spectrophotometer (Ocean Optics) under the excitation of a 980 nm laser (BWT Beijing, Ltd.). Fluorescence lifetime was measured with a spectrometer (Andor) equipped with a MDO3034 digital oscilloscope (Tektronix) under the 980 nm laser excitation. All the measurements were conducted at the room temperature.

DOI: 10.1021/acsami.9b16461
ACS Appl. Mater. Interfaces 2020, 12, 1292−1298

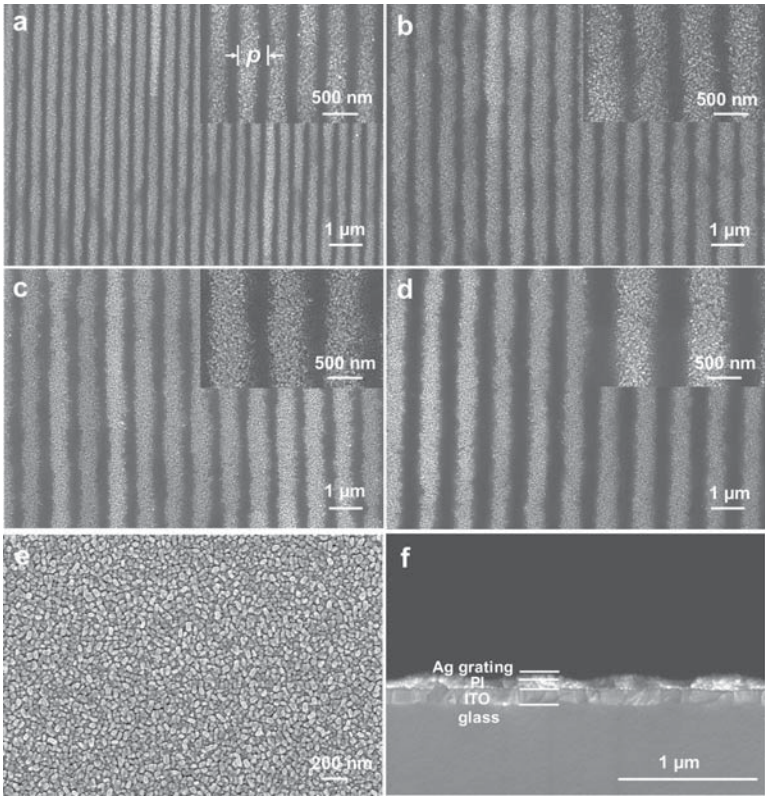

Figure 2. (a–d) Top-view SEM images of the fabricated Ag nanogratings. Insets are high magnification SEM images. (e) Top-view SEM image of the Ag nanofilm. (f) Cross-sectional view SEM image of the Ag nanograting structure with a period of 700 nm (in Figure 1b).

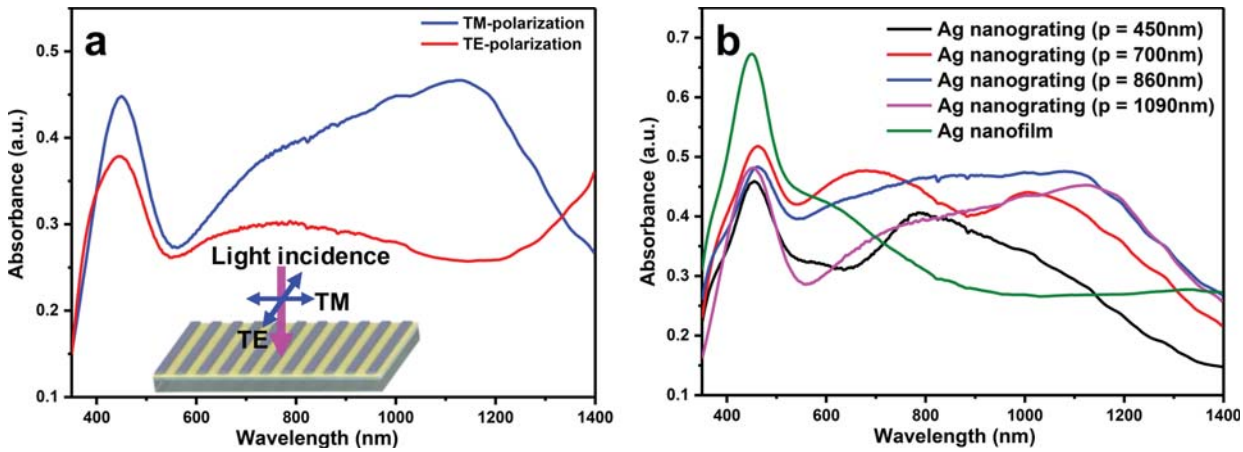

Figure 3. (a) Absorption spectra of the Ag nanograting with the period of 1090 nm under TM- and TE-polarized incident light. (b) Absorption spectra of the Ag nanogratings with different periods and the Ag nanofilm under TM-polarized incident light.

RESULTS AND DISCUSSION

Figure 2a–e shows the surface morphologies of Ag nanogratings and nanofilm, which were formed by the rod-like Ag nanocrystal aggregations, and Figure 2e clearly exhibits the average size of Ag nanocrystals of 68 nm in length and 36 nm in width. The top-view SEM images of Ag nanogratings show that the period of the Ag nanograting becomes large as the apex angle of the prisms increases. The measured periods of the fabricated Ag nanogratings were 450, 700, 860, and 1090 nm when the apex angles of the used prisms were 90°, 120°, 130°, and 140°, respectively. Figure 2f shows the cross-sectional SEM image of the Ag nanograting with a period of 700 nm, and the thickness of Ag nanograting is estimated to be ~62 nm.

As known, the metallic nanograting has polarization-dependent optical properties. We have therefore investigated the polarization-dependent absorption spectra of the fabricated Ag nanogratings. Figure 3a and Figure S-1 show the measured absorption spectra of one Ag nanograting with a period of 1090 nm, which illustrates a highly polarization-dependent absorption. Upon the TM-polarized incidence (polarization perpendicular to Ag nanograting lines), the absorption

DOI: 10.1021/acsami.9b16461
ACS Appl. Mater. Interfaces 2020, 12, 1292–1298

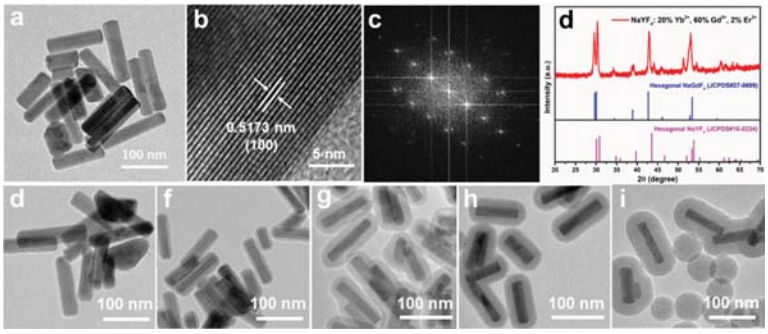

Figure 4. (a) TEM image, (b) HRTEM image, (c) FFT pattern, and (d) XRD spectrum of the $NaYF_4$:Gd^{3+}, Yb^{3+}, and Er^{3+} UCNRs. TEM images of core−shell UCNRs with different SiO_2 shell thicknesses of (e) 4, (f) 7, (g) 13.5, (h) 18.5, and (i) 23.5 nm.

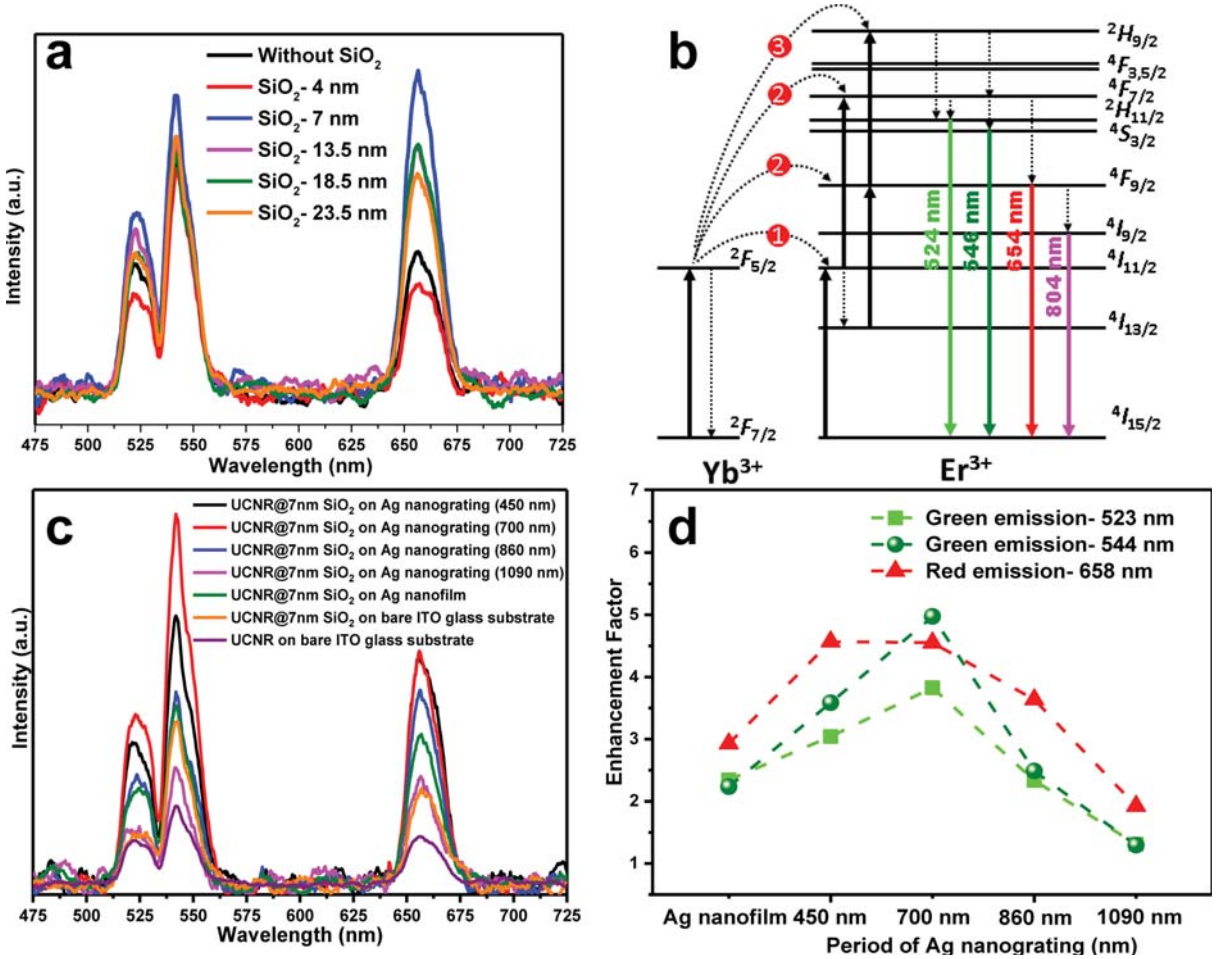

Figure 5. (a) PL spectra of UCNRs with different thickness of SiO_2 shell (0, 4, 7, 13.5, 18.5, and 23.5 nm) on the ITO glass substrates under a 980 nm laser excitation (625 mW/cm^2). (b) Schematic illustration of the energy transfer mechanism of Yb^{3+} and Er^{3+} in UCNRs. (c) PL spectra of the core−shell UCNRs@7nm SiO_2 on the Ag nanogratings with different periods, the Ag nanofilm, and the bare ITO glass substrate under the 980 nm laser excitation (625 mW/cm^2). (d) Enhancement factors of 523, 544, and 658 nm emission of Er^{3+} ions from the core−shell UCNRs on Ag nanogratings and nanofilm.

spectrum presents a narrow absorption band with a central wavelength of 447 nm, which is due to the LSPR of the Ag nanoparticles,[10,11,16] also a broadband absorption from 559 to 1400 nm, and the maximum absorption at 1134 nm under the incident light polarization parallel to grating structures. In contrast, upon the TE-polarized incidence (polarization parallel to Ag nanograting lines), the NIR broadband shows an abrupt decrease and the narrow absorption band of Ag grating also decreases slightly.[26] It clearly shows that the Ag nanograting has much stronger absorption for the TM-polarized incidence compared to the TE-polarized case. Figure 3b summarizes the measured absorption spectra for the Ag nanogratings with different periods and the Ag nanofilm under the TM-polarized incidence. We can see from Figure 3b that

DOI: 10.1021/acsami.9b16461
ACS Appl. Mater. Interfaces 2020, 12, 1292−1298

both the Ag nanogratings and nanofilm show a narrow absorption band at ~447 nm due to the LSPR of Ag nanoparticles; in addition, the Ag nanogratings possess a much broad absorption band in the range of 600−1400 nm that varies with the period. Overall, the broad absorption bands in the NIR region shows a tendency of red shift as the period of the Ag nanograting increases, which indicates that the absorption band can be well tuned via changing the period of the Ag nanograting. It is worth mentioning that the absorption of the Ag nanofilm does not show much polarization dependence as the Ag nanofilm is macroscopically isotropic. In addition, there is no remarkable intense NIR absorption band for the Ag nanofilm, further confirming that the NIR broadband absorption mainly arises from the periodic Ag nanograting.

On the other hand, the $NaYF_4$:Gd^{3+}, Yb^{3+}, and Er^{3+} UCNRs were synthesized via a hydrothermal method and their morphology and phase structure are shown in Figure 4a−d. The TEM image in Figure 4a exhibits the synthesized product consisting of dispersive rod-shape nanocrystals with an average size of 103 nm in length and 24 nm in width. The HRTEM image in Figure 4b reveals clear crystal lattice fringes with a spacing of 0.5173 nm, corresponding to (100) of the hexagonal phase $NaYF_4$. Figure 4c shows the fast Fourier transform (FFT) pattern based on the HRTEM image, indicating an excellent and single crystalline quality based on the clear lattice diffraction pattern. Moreover, the XRD pattern in Figure 4d shows that all the diffraction peaks in the patterns could be indexed to the standard card of $NaYF_4$ (JCPDS no. 16-0334) but a slight blue shift for the large amount (60%) of Gd^{3+} doping ($NaGdF_4$ (JCPDS no. 27-0699)) into the crystal lattice. Furthermore, with results from the EDS spectrum and two-dimensional mapping distribution images in Figure S-2, the product mainly consists of Na, Y, Gd, Yb, Er, and F elements, which are evenly distributed in the hexagonal phase $NaYF_4$ matrix nanocrystals. In addition, the mass fraction of these elements is summarized in Table S-1. There exists a slight difference in the fractions of these elements between the designed and measured results, which is reasonable by considering some ion losses in the sample preparation. Based on the previous reports,[11,12,16,25] the gap between UCNPs and plasmonic structures is of great importance on tuning the plasmonic enhancement effect and alleviating the quenching effect. Figure 4e−i shows the UCNRs coated with SiO_2 shells of thickness varying from 4, 7, 13.5, 18.5, to 23.5 nm, and the appearance of SiO_2 nanospheres in Figure 4i is due to the excess amount of TEOS. In addition, the XRD pattern (Figure S-3) of UCNR@SiO_2 nanocrystals contains the typical diffraction peaks of $NaYF_4$ as well as a broad diffuse scattering band centered at $2\theta \approx 22°$, indicating the existence of the amorphous SiO_2 in the sample. The EDS spectrum of UCNR@SiO_2 nanocrystals in Figure S-4 also confirms the existence of the Si and O elements in the sample. In addition, the XPS results in Figure S-5 demonstrate that the 2p level of Si at 103 eV appears in UCNR@SiO_2 nanocrystals compared with that in UCNR, which is coincident with the EDS results. The FTIR spectrum (Figure S-6) of the UCNR@SiO_2 sample shows an obvious peak at 1093 cm^{-1} that belongs to Si−O−Si bending vibration from the SiO_2-coating layers. Moreover, TGA curves (Figure S-7) show a weight loss from 25 to 590 °C for both UCNR and UCNR@SiO_2 due to the removal of the hydroxyl and oleate compounds on the surface. DLS analysis (Figure S-8) shows the sharp peaks for both UCNR and UCNR@SiO_2 samples, indicating the nanocrystals are well dispersed in the solution without obvious aggregation. In addition, due to the SiO_2 shell coating, the UCNR@SiO_2 core−shell structures present a larger volume-average hydrodynamic size (340 nm) than that (190 nm) in the oleic-coated UCNR. Also, the result in Figure S-9 shows that UCNR@SiO_2 nanocrystals are negatively charged in ethanol with an average zeta potential of about −30.3 mV. These results further confirm the effective SiO_2 coating on the surface of UCNR nanocrystals. Both UCNR and UCNR@SiO_2 samples have a good stability and dispersity in ethanol for use.

Figure 5a shows the PL spectra of $NaYF_4$:Gd^{3+}, Yb^{3+}, and Er^{3+} UCNRs with different thicknesses of the SiO_2 shell (0, 4, 7, 13.5, 18.5, and 23.5 nm) on an ITO glass substrate under excitation of a 980 nm laser (625 mW/cm^2), which show the characteristic peaks of Er^{3+}: 523 nm ($^2H_{11/2} \rightarrow {}^4I_{15/2}$), 544 nm ($^4S_{3/2} \rightarrow {}^4I_{15/2}$), and 658 nm ($^4F_{9/2} \rightarrow {}^4I_{15/2}$). The schematic illustration of the energy transfer (ET) mechanism of Yb^{3+} and Er^{3+} in UCNRs is shown in Figure 5b. The Er^{3+} ions are excited to the $^4F_{7/2}$ and $^4F_{9/2}$ states via the Yb^{3+}-assisted two photon ET processes, descending to the lower level of $^2H_{11/2}$, $^4S_{3/2}$, and $^4F_{9/2}$ through a series of nonradiative relaxation process and finally giving out the green and red emission of Er^{3+} via radiative relaxation. In addition, we can see from Figure 5a that compared to the UCNRs without a SiO_2 shell, the UCL intensities of UCNRs with a shell thickness of larger than 4 nm are enhanced due to the passivation of surface defects, while there is a slight decrease in UCL intensity for a shell thickness of 4 nm since the SiO_2 shell is too thin to inactivate the defects.[25] For the enhancement case, the UCL intensity first increases and then decreases with the increase of the shell thickness. In our experiments, the UCNRs with a SiO_2 shell thickness of 7 nm demonstrated the strongest UCL intensity, which were chosen for the further investigation. The core−shell UCNRs with a shell thickness of 7 nm were spin-coated on the Ag nanogratings with different periods. The cross-sectional SEM image of the structure is shown in Figure S-10, and the UCNRs@7nm SiO_2 layer is around 500 nm. The corresponding PL spectra of UCNRs@7nm SiO_2 on different Ag nanogratings and nanofilm are shown in Figure 5c. Compared to that in the core−shell UCNRs on the bare ITO glass, the UCL of Er^{3+} shows an obvious enhancement on the Ag nanogratings, which could be mainly attributed to the plasmonically enhanced absorption of the excitation laser light and the electric field enhancement induced by the LSPR of Ag nanocrystals. Meanwhile, the UCL of Er^{3+} on the Ag nanofilm could be ascribed to the LSPR of Ag nanocrystals and the SPP of the film. We also found that with the increased period of the Ag nanogratings, the UCL intensity increases first and then decreases. The strongest UCL intensity was achieved with the period of the Ag nanograting of 700 nm. From Figure 5c,d, we can see that the enhancement factor of UCL from the Ag nanograting (a period of 700 nm) is about two times higher than that from the Ag nanofilm. From Figure 3b, we can observe much stronger and broader NIR absorption from the Ag nanograting compared to the Ag nanofilm. Therefore, in addition to LSPR-enhanced emission caused by the Ag nanocrystals from both Ag nanogratings and nanofilms, we have attributed the UCL enhancement from the UCNRs on the Ag nanograting significantly to the plasmonically enhanced NIR absorption of the periodic Ag nanograting. To confirm this proposed mechanism, the fluorescence lifetime was further measured. Under excitation of a 980 nm laser, the fluorescence

DOI: 10.1021/acsami.9b16461
ACS Appl. Mater. Interfaces 2020, 12, 1292−1298

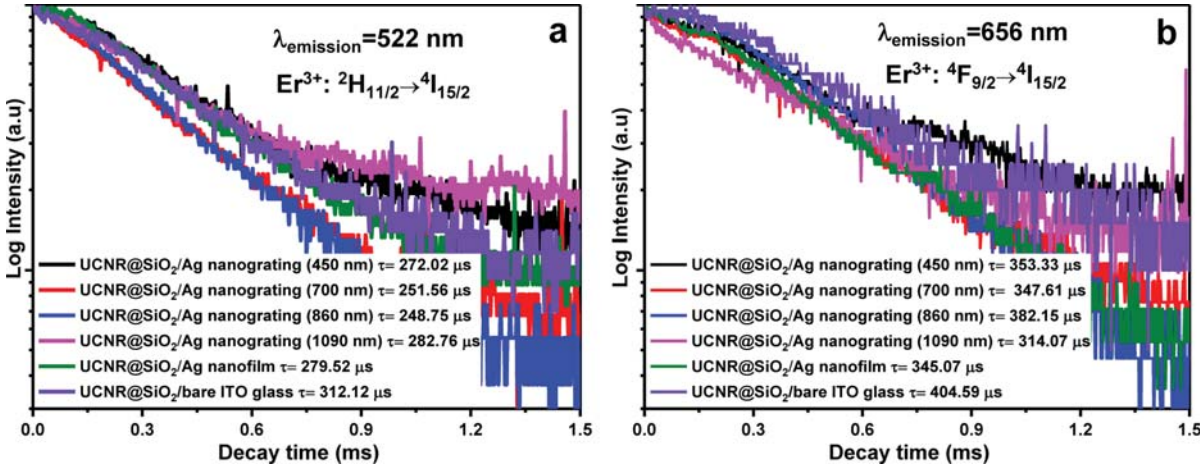

Figure 6. Fluorescence decay curves of Er^{3+} emission at (a) 522 nm ($^2H_{11/2} \rightarrow {}^4I_{15/2}$) and (b) 656 nm ($^4F_{9/2} \rightarrow {}^4I_{15/2}$) from the core−shell UCNRs@7nm SiO_2 on the Ag nanogratings, Ag nanofilm, and bare ITO glass substrate under the 980 nm laser excitation.

decay curves of Er^{3+} emission at 522 nm ($^2H_{11/2} \rightarrow {}^4I_{15/2}$) and 656 nm ($^4F_{9/2} \rightarrow {}^4I_{15/2}$) from UCNRs@7nm SiO_2 on the Ag nanogratings and nanofilm show an obvious decrease in Figure 6, compared to the case of the UCNRs@7nm SiO_2 on the bare ITO glass substrate, which further confirms that the LSPR of Ag nanocrystals results in the emission enhancement since the radiation transition rate of Er^{3+} in UCNRs enhances greatly with the introduction of Ag nanogratings or nanofilm, leading to an enhancement emission intensity but a decrease in fluorescent lifetime.[17] Furthermore, Figure 5d shows EFs of 523, 544, and 658 nm emission of Er^{3+} ions from the core−shell UCNRs on different Ag plasmonic structures. The maximum EFs of 523 nm, 544 nm (green emission), and 658 nm (red emission) of Er^{3+} ions are 3.8-, 5.5-, and 4.6-folds, respectively, and the overall UC emission can be enhanced by around 4.5 times. Thus, the holographically synthesized Ag nanogratings have comparable performance in UCL enhancement due to the grating-induced absorption and LSPRs compared to previously reported results.[21] More importantly, in terms of ease of design and fabrication, our approach presents a cost-effective, high-throughput way to holographically synthesize the Ag nanogratings with different periods, compared to those template-assisted deposition or lithographic methods.[20,21]

CONCLUSIONS

In summary, we have demonstrated that the UCL can be greatly enhanced by integrating the core−shell UCNRs with the Ag nanogratings. Both the Ag nanogratings and UCNRs can be fabricated/synthesized in a facile, cost-effective, high-throughput way. Our experimental results have shown that the UCL intensity of Er^{3+} in the core−shell UCNRs can be tuned and enhanced by changing the SiO_2 shell thickness and the period of the Ag nanograting. The underlying physical mechanism for the UCL enhancement can be attributed to the plasmonically enhanced NIR broadband absorption of the periodic Ag nanograting and the LSPR of Ag nanocrystals. The maximum EFs of 523 nm, 544 nm (green emission), and 658 nm (red emission) of Er^{3+} ions excited at 980 nm are 3.8, 5.5, and 4.6-folds, respectively. Our fabrication approach and results suggest that such a simple integration could make the enhanced UCL practical for biosensing/imaging and anti-counterfeiting applications.

ASSOCIATED CONTENT

Supporting Information

The Supporting Information is available free of charge at https://pubs.acs.org/doi/10.1021/acsami.9b16461.

Figures S-1 to S-10 and Table S-1 describe the characterization of absorption, distribution mapping and mass fraction of elements, EDS, XRD, XPS, FTIR, TGA, DLS, zeta potential, SEM images of the synthesized UCNPs and Ag nanogratings (PDF)

AUTHOR INFORMATION

Corresponding Authors

*E-mail: gcxing@um.edu.mo (G.X.).
*E-mail: yjliu@sustech.edu.cn (Y.J.L.).

ORCID

Dan Luo: 0000-0003-2117-0570
Rui Chen: 0000-0002-0445-7847
Guichuan Xing: 0000-0003-2769-8659
Yan Jun Liu: 0000-0001-8724-0434

Author Contributions

⊥A.C. and H.H. contributed equally to this work.

Notes

The authors declare no competing financial interest.

ACKNOWLEDGMENTS

This work was supported in part by National Natural Science Foundation of China (grant no. 61805113), Natural Science Foundation of Guangdong Province (grant nos. 2017A030313034 and 2018A030310224), Guangdong Innovative and Entrepreneurial Research Team Program (grant no. 2017ZT07C071), and Shenzhen Science and Technology Innovation Commission (grant nos. JCYJ20170817111349280, JCYJ20180305180635082, and KQTD2016030111203005). G.X. acknowledges financial support from the Science and Technology Development Fund (file no. 116/2016/A3, 091/2017/A2, 014/2017/AMJ), the Research Grant (SRG2016-00087-FST, MYRG2018-00148-IAPME) from University of Macau, and

DOI: 10.1021/acsami.9b16461
ACS Appl. Mater. Interfaces 2020, 12, 1292−1298

the Natural Science Foundation of China (91733302, 61605073, 2015CB932200).

REFERENCES

(1) Zhou, B.; Shi, B.; Jin, D.; Liu, X. Controlling Upconversion Nanocrystals for Emerging Applications. *Nat. Nanotechnol.* **2015**, *10*, 924−936.
(2) Li, X.; Zhang, F.; Zhao, D. Lab on Upconversion Nanoparticles: Optical Properties and Applications Engineering via Designed Nanostructure. *Chem. Soc. Rev.* **2015**, *44*, 1346−1378.
(3) Wang, D.; Liu, B.; Quan, Z.; Li, C.; Hou, Z.; Xing, B.; Lin, J. New Advances on the Marrying of UCNPs and Photothermal Agents for Imaging-guided Diagnosis and the Therapy of Tumors. *J. Mater. Chem. B* **2017**, *5*, 2209−2230.
(4) Yuan, Y.; Xu, L.; Dai, S.; Wang, M.; Wang, H. A Facile Supramolecular Approach to Fabricate Multifunctional Upconversion Nanoparticles as a Versatile Platform for Drug Loading, in Vivo Delivery and Tumor Imaging. *J. Mater. Chem. B* **2017**, *5*, 2425−2435.
(5) Das, A.; Mao, C.; Cho, S.; Kim, K.; Park, W. Over 1000-fold Enhancement of Upconversion Luminescence Using Water-dispersible Metal-insulator-metal nanostructures. *Nat. Commun.* **2018**, *9*, 4828.
(6) Wen, H.; Zhu, H.; Chen, X.; Hung, T. F.; Wang, B.; Zhu, G.; Yu, S. F.; Wang, F. Upconverting Near-infrared Light Through Energy Management in Core-shell-shell Nanoparticles. *Angew. Chem., Int. Ed.* **2013**, *52*, 13419−13423.
(7) He, H.; Zhang, Y.; Li, Y.; Wang, L.; Gao, X.; Zhang, X.; He, D.; Chen, R.; Luo, D.; Sun, X. W.; Liu, Y. J. Facile Synthesis and Controllable Emission of Tm^{3+}/Er^{3+}-Doped and -Co-doped α-$NaYbF_4$Upconversion Nanocrystals. *ACS Omega* **2018**, *3*, 17814−17820.
(8) Lin, X.; Chen, X.; Zhang, W.; Sun, T.; Fang, P.; Liao, Q.; Chen, X.; He, J.; Liu, M.; Wang, F.; Shi, P. Core-Shell-Shell Upconversion Nanoparticles with Enhanced Emission for Wireless Optogenetic Inhibition. *Nano Lett.* **2018**, *18*, 948−956.
(9) Yin, Z.; Li, H.; Xu, W.; Cui, S.; Zhou, D.; Chen, X.; Zhu, Y.; Qin, G.; Song, H. Local Field Modulation Induced Three-Order Upconversion Enhancement: Combining Surface Plasmon Effect and Photonic Crystal Effect. *Adv. Mater.* **2016**, *28*, 2518−2525.
(10) Feng, W.; Sun, L.-D.; Yan, C.-H. Ag Nanowires Enhanced Upconversion Emission of $NaYF_4$:Yb,Er Nanocrystals via a Direct Assembly Method. *Chem. Commun.* **2009**, *29*, 4393−4395.
(11) Yin, D.; Wang, C.; Ouyang, J.; Zhang, X.; Jiao, Z.; Feng, Y.; Song, K.; Liu, B.; Cao, X.; Zhang, L.; Han, Y.; Wu, M. Synthesis of a Novel Core-shell Nanocomposite $Ag@SiO_2@Lu_2O_3$:Gd/Yb/Er for Large Enhancing Upconversion Luminescence and Bioimaging. *ACS Appl. Mater. Interfaces* **2014**, *6*, 18480−18488.
(12) He, J.; Zheng, W.; Ligmajer, F.; Chan, C.-F.; Bao, Z.; Wong, K.-L.; Chen, X.; Hao, J.; Dai, J.; Yu, S.-F.; Lei, D. Y. Plasmonic Enhancement and Polarization Dependence of Nonlinear Upconversion Emissions from Single Gold Nanorod@SiO_2@CaF_2:Yb^{3+},Er^{3+} Hybrid Core-shell-satellite Nanostructures. *Light: Sci. Appl.* **2017**, *6*, No. e16217.
(13) Liu, J.; He, H.; Xiao, D.; Yin, S.; Ji, W.; Jiang, S.; Luo, D.; Wang, B.; Liu, Y. Recent Advances of Plasmonic Nanoparticles and their Applications. *Materials* **2018**, *11*, 1833.
(14) Park, K.; Park, M.; Jang, H. S.; Park, J. H.; Kim, J.; Cho, Y.; Han, I. K.; Byun, D.; Ko, H. Highly Secure Plasmonic Encryption Keys Combined with Upconversion Luminescence Nanocrystals. *Adv. Funct. Mater.* **2018**, *28*, 1800369.
(15) Chen, X.; Xu, W.; Zhang, L.; Bai, X.; Cui, S.; Zhou, D.; Yin, Z.; Song, H.; Kim, D.-H. Large Upconversion Enhancement in the "Islands" Au-Ag Alloy/$NaYF_4$: Yb^{3+}, Tm^{3+}/Er^{3+} Composite Films, and Fingerprint Identification. *Adv. Funct. Mater.* **2015**, *25*, 5462−5471.
(16) Yuan, P.; Lee, Y. H.; Gnanasammandhan, M. K.; Guan, Z.; Zhang, Y.; Xu, Q.-H. Plasmon Enhanced Upconversion Luminescence of NaYF4:Yb,Er@SiO_2@Ag Core-shell Nanocomposites for Cell Imaging. *Nanoscale* **2012**, *4*, 5132−5137.
(17) Kwon, S. J.; Lee, G. Y.; Jung, K.; Jang, H. S.; Park, J. S.; Ju, H.; Han, I. K.; Ko, H. A Plasmonic Platform with Disordered Array of Metal Nanoparticles for Three-Order Enhanced Upconversion Luminescence and Highly Sensitive Near-Infrared Photodetector. *Adv. Mater.* **2016**, *28*, 7899−7909.
(18) Park, K.; Jung, K.; Kwon, S. J.; Jang, H. S.; Byun, D.; Han, I. K.; Ko, H. Plasmonic Nanowire-Enhanced Upconversion Luminescence for Anticounterfeit Devices. *Adv. Funct. Mater.* **2016**, *26*, 7836−7846.
(19) Li, A.-H.; Lü, M.; Guo, L.; Sun, Z. Enhanced Upconversion Luminescence of Metal-Capped $NaGd_{0.3}Yb_{0.7}F_4$:Er Submicrometer Particles. *Small* **2016**, *12*, 2092−2098.
(20) Xu, W.; Song, H.; Chen, X.; Wang, H.; Cui, S.; Zhou, D.; Zhou, P.; Xu, S. Upconversion Luminescence Enhancement of Yb^{3+}, Nd^{3+} Sensitized $NaYF_4$ Core-shell Nanocrystals on Ag Grating Films. *Chem. Commun.* **2015**, *51*, 1502−1505.
(21) Lu, D.; Cho, S. K.; Ahn, S.; Brun, L.; Summers, C. J.; Park, W. Plasmon Enhancement Mechanism for the Upconversion Processes in $NaYF_4$:Yb^{3+},Er^{3+} Nanoparticles: Maxwell versus Förster. *ACS Nano* **2014**, *8*, 7780−7792.
(22) Liu, Y. J.; Sun, X. W.; Liu, J. H.; Dai, H. T.; Xu, K. S. A Polarization Insensitive 2×2 Optical Switch Fabricated by Liquid Crystal-Polymer Composite. *Appl. Phys. Lett.* **2005**, *86*, 041115.
(23) Lu, M.; Juluri, B. K.; Zhao, Y.; Liu, Y. J.; Bunning, T. J.; Huang, T. J. Single-step Holographic Fabrication of Large-area Periodically Corrugated Metal Films. *J. Appl. Phys.* **2012**, *112*, 113101−113106.
(24) Wang, F.; Han, Y.; Lim, C. S.; Lu, Y.; Wang, J.; Xu, J.; Chen, H.; Zhang, C.; Hong, M.; Liu, X. Simultaneous Phase and Size Control of Upconversion Nanocrystals through Lanthanide Doping. *Nature* **2010**, *463*, 1061−1065.
(25) Rohani, S.; Quintanilla, M.; Tuccio, S.; De Angelis, F.; Cantelar, E.; Govorov, A. O.; Razzari, L.; Vetrone, F. Enhanced Luminescence, Collective Heating, and Nanothermometry in an Ensemble System Composed of Lanthanide-Doped Upconverting Nanoparticles and Gold Nanorods. *Adv. Opt. Mater.* **2015**, *3*, 1606−1613.
(26) Wang, W.; Hao, Y.; Cui, Y.; Zhang, Y.; Shi, F.; Wei, B.; Huang, W. Ultra-Thin Organic Solar Cells Incorporating Dielectric-Coated Comb Silver Nanogratings. *Plasmonics* **2016**, *11*, 151−157.

DOI: 10.1021/acsami.9b16461
ACS Appl. Mater. Interfaces 2020, 12, 1292−1298